

Synthesis of Nano-Calcium Fluoride – Based Materials from Phosphogypsum Waste and their Use in Wastewater Treatment – Adsorption of Reactive Blue 21 Dyes

Meryem Bensemlali^{1*}, Badreddine Hatimi¹, Halima Mortadi², Fatima-Zahra Chajri¹, Abdellatif Aarfane^{1,3}, El Idrissi Mohammed⁴, Meryeme Joudi¹, Najoua Labjar⁵, Hamid Nasrellah^{1,3}, Mina Bakasse¹

¹ Laboratory of Organic Bioorganic and Environmental Chemistry, Chouaib Doukkali University, Morocco

² Faculty of Sciences, University Chouaib Doukkali, Chemistry Department, Laboratory of Materials' Physical, Chemicals, El Jadida, Morocco

³ Higher School of Education and Training, Chouaib Doukkali University, Morocco

⁴ Laboratory of Chemical Processes and Applied Materials, Polydisciplinary Faculty, Sultan Moulay Slimane University, Beni-Mellal, Morocco

⁵ Laboratory of Spectroscopy, Molecular Modelling, Materials, Nanomaterials, Water and Environment, ENSAM University Mohammed V in Rabat, Morocco

* Corresponding author's e-mail: bensemlali.meryem@gmail.com

ABSTRACT

A novel synthesis process and characterization of nano-calcium fluoride (n-CaF₂) single crystal prepared from phosphogypsum waste. The phosphogypsum (CaSO₄·2H₂O) powder has been mechanically mixed with NH₄F in presence of a controlled amount of water. The mixture still sintered for 48 hours until the formation of nano calcium fluoride particles. The n-CaF₂ particles have been characterized by several techniques, The techniques utilized included X-ray diffraction (XRD), infrared spectroscopy (IR), and scanning electron microscopy (SEM). Therefore, it was confirmed that very pure n-CaF₂ was obtained with a Ca/F ratio of 0.5 and an average crystalizing size measured according to the Debye-Scherrer equation of 11 nm. Based on the findings reached, The characterization data revealed successful synthesis of n-CaF₂ from phosphogypsum. Additionally, the adsorption performance of the elaborated n-CaF₂ was tested in Reactive Blue 21 (RB21) anionic dye removal, Adsorption tests were conducted in a batch reactor, focusing on key factors such as contact time, which can significantly influence the adsorption results. adsorption amount, pH, and dye concentration were tested. Hence results show an important adsorption performance of n-CaF₂ with Reactive Blue 21 removal rate up to 90%.

Keywords: phosphogypsum waste; nano-calcium fluoride; wastewater; Reactive Blue 21 adsorption.

INTRODUCTION

Mineral wastes are hazardous material that can cause several issues to the environmental system, consequently it become an obligation to recycle a such materials. Nowadays, synthesis of nanomaterials from inorganic residues consists of a promising way for valuing those wastes. Phosphogypsum's environmental impact stems from its toxicity and large-scale production, leading

to various damages. However, recognizing phosphogypsum as a calcium source can have profound implications across scientific disciplines like biology, chemistry, health, medicine, and even biomineralization studies (Motameni et al., 2021, Fosca et al., 2022, Zhou et al., 2021, Jang et al., 2023, Golubchikov et al., 2023, Young et al., 2008). The most commonly extracted forms of phosphogypsum are calcium phosphate phases, which can be synthesized into biofunctional

materials like hydroxyapatite for various applications (HA, $\text{Ca}_{10}(\text{PO}_4)_6(\text{OH})_2$) (Nasrellah et al., 2017), fluoroapatite (FA, $\text{Ca}_{10}(\text{PO}_4)_6(\text{F})_2$) (Nasrellah et al., 2022), anhydrous dicalcium phosphate (DCPA, CaHPO_4) (Yassine et al., 2022), Amorphous calcium phosphate (ACP), tetra calcium phosphate (TTCP, $\text{Ca}_4(\text{PO}_4)_2\text{O}$), dicalcium phosphate dihydrate (DCPD, $\text{CaHPO}_4 \cdot 2\text{H}_2\text{O}$), and nanocalcite CaCO_3 are calcium-based compounds discussed in Bensemali et al. (2022) study. These compounds are notable for their distinctive properties and potential uses in various applications. Recycling phosphogypsum waste into nanomaterials is a common practice across different fields, with n- CaF_2 standing out as an appealing choice for host crystals in specific applications.

The aim purpose of this work consisted in ensuring whether these materials were suitable for use as effective laser-pumped amplifier media. Besides, calcium fluoride (CaF_2) based materials are taking a significant interest in dentistry due to the role that they play as labile fluoride (F) reservoirs in cavities prevention. Furthermore, low concentration of fluor used in oral fluids derived as reservoirs formed using dentifrices and rinses have been proved to profound effect on the progression of dental cavities (Mayerhöfer et al., 2020, Mitwalli et al., 2022, Matsuo et al., 1990, Rølla et al., 1990). Few studies have been conducted on the synthesis of fluoride nanoparticles, and the available data in the literature are limited. However, it has been demonstrated that CaF_2 nanoparticles can be synthesized using various methods, including sol-gel (Fujihara et al., 2002, Zhou et al., 2007), solvothermal processes (Kumar et al., 2007), reverse micelle methods (Bensalah et al., 2006), different precipitation methods (Sun et al., 2003, Mortier et al., 2007, Wang et al., 2007), and flame synthesis (Grass et al., 2005, Bhadane et al., 2023, Takaya et al., 2021, and Kumar et al., 2022).

In the present study, we propose a novel method for n- CaF_2 elaboration based on phosphogypsum. This method is simple, doesn't require much energy, and additionally can easily be industrialized (Wu et al., 1994, Wang 2023). The CaF_2 nanoparticles are prepared by precipitation method while mechanical stirring was utilized. The synthesis was carried out in reactor where the appropriate amount of anhydrite, and the same Mass in NH_4F has been mixed and agitated for 48 Hours. During the reaction, a progressive transformation of mixer to a white opaque suspension was noted. Then, the mixture is centrifuged and

washed with water to eliminate the residual sulphate and the ammonium ions. Finally, the collect solid was characterized by XRD, SEM, IR techniques. Accordingly, it was confirmed that the solid consists of a case pure fluorine with crystalline size of 11 nm. Later the elaborated n- CaF_2 was deployed for Reactive Blue 21 anionic dye (RB21) removal. The material shows an important dye elimination performance that reach 90% in the optimal condition of pH, adsorbent amount, day concentration and constant time.

MATERIALS AND METHODS

Raw materials

Phosphogypsum (PG) samples were obtained from a Moroccan phosphate industry in Morocco. The chemical composition of PG was determined using ICP analysis, and the results are presented in Table 1. The analysis revealed that PG is primarily composed of calcium (Ca) and sulfur (S), with lower amounts of phosphorus (P), aluminum (Al), iron (Fe), potassium (K), fluorine (F), magnesium (Mg), sodium (Na), and silicon (Si).

The dye used in this study is Reactive Blue 21. The RB 21 is an anionic dye negatively charged. Table 2 summarize the mains characteristics of RB 21.

Pre-treatment of phosphogypsum

The phosphogypsum is treated with sulfuric acid of 67% purity in order to remove soluble impurities and heavy metals and to dehydrate the phosphogypsum to anhydrite.

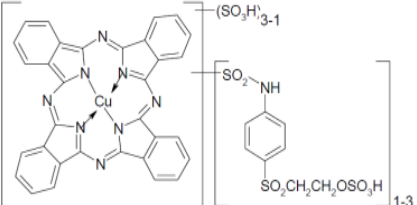
Synthesis of stoichiometric n- CaF_2 powder

The method of preparing n- CaF_2 is detailed in Figure 1. Initially, a solution of 67% sulfuric acid was added to 300 g of phosphogypsum in water. This mixture was then placed in a custom-made reactor, vigorously stirred at 50 °C for 45 minutes, and subsequently filtered to obtain anhydrite. Following this, 200 g of the obtained anhydrite was combined with 109 g of pure NH_4F and 2 L of distilled water. The resulting mixture was stirred mechanically at 500 rpm for 48 hours until a white suspension formed. The suspension was then separated, washed with distilled water, dried at 105 °C, and calcined at temperatures ranging from 600 °C to 900 °C for 3 hours. The resulting powder comprised stoichiometric n- CaF_2 . The

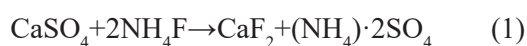
Table 1. Chemical composition of phosphogypsum from moroccan phosphate industry (weight %)

Ca	S	P	C	Al	Fe	K	F	Mg	Na	Si
23.05	18.04	0.40	0.14	0.07	0.58	0.14	0.12	0.10	0.10	0.25

Table 2. Characteristics of the studied dye

Dye	λ_{max}	Molar mass g/mol	Chemical structure
Reactive Bleu 21 (anionic)	620 nm	1083.5	

reaction for the formation of nano n-CaF₂ can be expressed as follows:



Materials characterizations

The mineralogy of n-CaF₂ was thoroughly investigated through a range of analytical methods. X-ray diffraction (XRD) analysis was performed using a XRD Pert Pro MPD instrument from P-analytical, utilizing Cu K α radiation with a wavelength of 1.54 Å. The XRD scans were conducted at a scanning rate of 0.02°/s over a 2 θ range of 5–80°. Scanning electron microscopy (SEM) was carried out using an FEI Quanta 200 ESEM instrument to visualize the morphology of the samples. Thermal analysis was

conducted through gravimetric analysis to understand the thermal behavior of the material. Infrared spectroscopy (FTIR) was employed using an FTIR-8400S instrument to analyze the chemical bonds and functional groups present. Additionally, Inductively Coupled Plasma (ICP) analysis was performed using an AES Jobin Yvon Ultima 2 instrument to determine the elemental composition of the material. These combined techniques provided a comprehensive understanding of the mineralogical and chemical characteristics of the synthesized n-CaF₂ material.

Adsorption of Reactive Bleu 21 into n-CaF₂

The adsorption tests were conducted using a batch reactor, where colored synthetic solutions

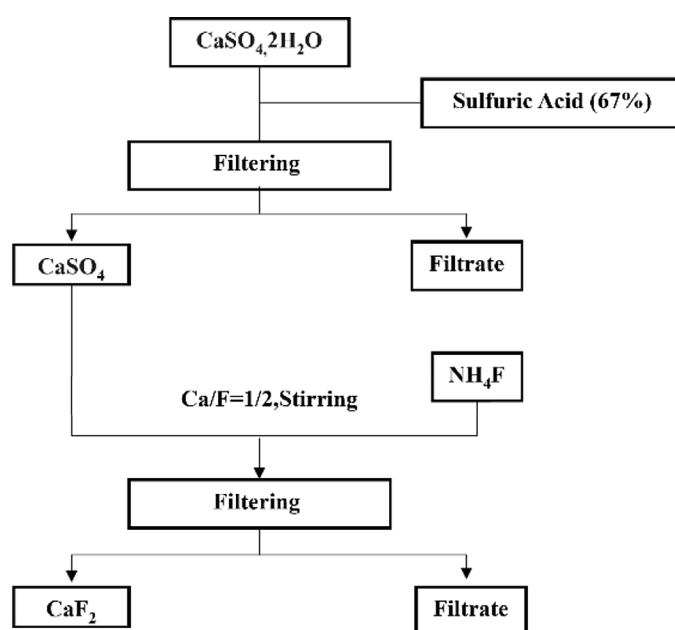


Figure 1. Diagram of preparing n-CaF₂ particles from natural phosphogypsum

were stirred in the presence of synthesized calcium fluoride (CaF_2). We investigated the impact of key parameters on adsorption capacity, including adsorbent mass, medium pH, contact time, and initial dye concentration. The residual concentration of each dye was measured using a Jasco 620 UV-visible spectrophotometer. Absorbance readings were taken after centrifuging the treated solution at 4000 rpm. Residual dye content was determined by interpolating the results using a previously established calibration curve. The tests involved shaking 100 mL of a 20 mg/L dye solution with varying masses of synthesized CaF_2 (ranging from 0.1 to 1.1 g) in 250 mL containers. The resulting mixture was stirred at 500 rpm for 2 hours at a temperature of 25 °C and an initial pH of 6.4. The supernatants were then analyzed to assess dye yield relative to the added adsorbent mass.

RESULTS AND DISCUSSION

Characterization of n- CaF_2

XRD-diffraction

Figure 2 illustrates the X-ray diffraction (XRD) patterns of n- CaF_2 particles obtained from Moroccan phosphogypsum at temperatures of 105 °C, 600 °C, and 900 °C. The diffraction peaks observed in the XRD patterns correspond to the characteristic peaks of pure cubic structural n- CaF_2 , as indicated by JCPDS card 87–0971. The XRD patterns of CaF_2 nanoparticles are depicted in Figure 2. All diffraction

peaks correspond to a pure cubic phase with space group Fm-3m (225), in agreement with the standard values for cubic CaF_2 based on JCPDS Card no. 87–0971 (Gerward et al., 1992). These XRD results confirm that the synthesized products are composed of CaF_2 nanoparticles. For estimating the crystallite size, we can use Scherrer's formula, which provides a simple evaluation of the order of magnitude of the average crystallite size. This calculation is summarized in Table 3 (Zsigmondy et al., 1912):

$$D = \frac{k\lambda}{\beta \cos\theta} \quad (2)$$

The results confirm that the average grain size increases with the sintering temperature, as shown in Figure 3. Specifically, the particle diameter increases from 11.22 nm at 105 °C to 51.55 nm at 600 °C, and further to 68.27 nm at 900 °C (Alzahrani et al., 2022).

Fourier transform infrared spectrum (FTIR)

The purity of the synthesized CaF_2 , despite being a white powder, was further assessed using FT-IR spectrometry. Figure 4 displays the infrared absorption spectra of n- CaF_2 powders before and after heat treatment at 600 °C and 900 °C. In the FT-IR spectrum shown in Figure 3, the peak observed at 443 cm^{-1} is attributed to the Ca-F stretching vibration of CaF_2 . Additionally, the spectrum exhibits a strong IR absorption band at 3423 cm^{-1} , corresponding to the H-O-H bending of H_2O molecules. Therefore, the presence of hydroxyl groups in the as-prepared nanoparticle can be confirmed. (Lebkiri et al., 2023).

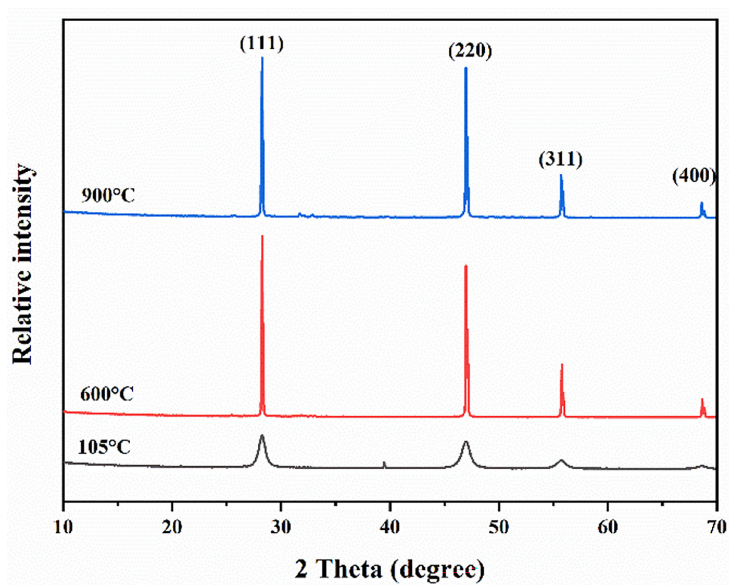


Figure 2. XRD patterns of n- CaF_2 dried at: (a) 105 °C, calcined at (b) 600 °C, and 900 °C (c)

Table 3. values of particle size of n-CaF₂ based on the Scherrer formula

Temperature, °C	D (nm)
105	11.22
600	51.20
900	68.27

Scanning electron microscopy of n-CaF₂ obtained

Figure 6 illustrates that the materials formed during the precipitation process consist of much smaller particles, which then agglomerate into larger structures measuring a few microns. Furthermore, an increase in the calcination temperature leads to an increase in particle size, accompanied by a transformation in crystal shape to a more rounded form. This observation is supported by X-ray diffraction analysis, which shows a very fine peak indicating the effect of temperature on crystallinity.

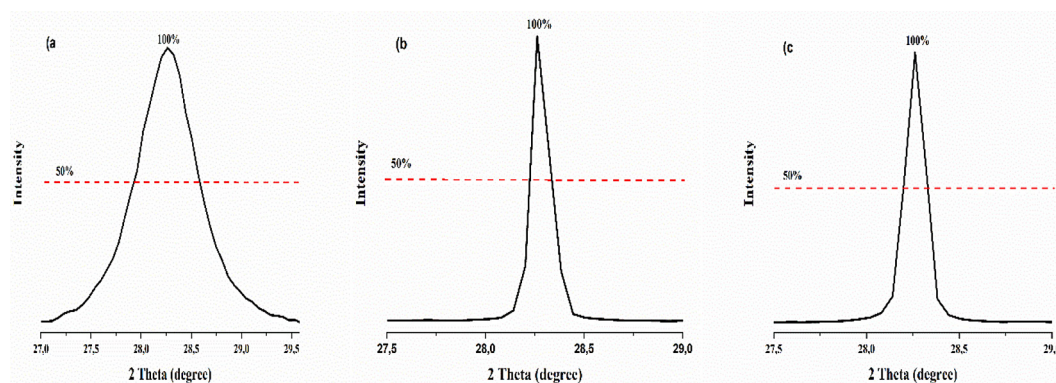
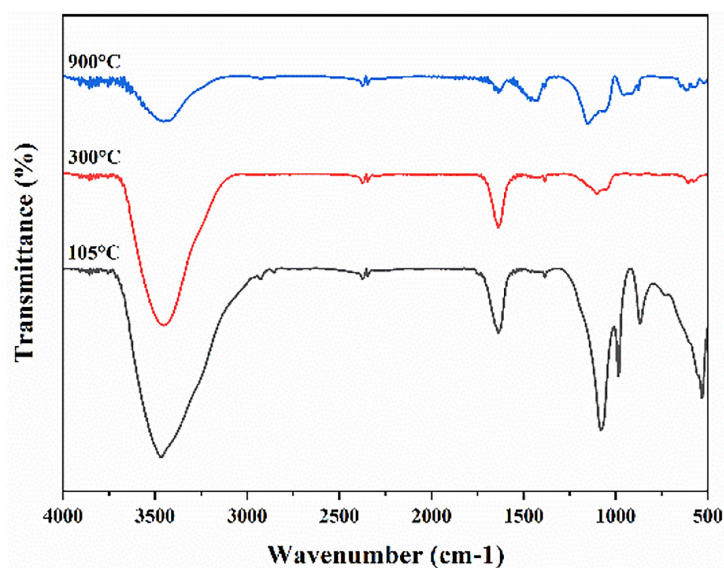
Inductively coupled plasma of n-CaF₂ particles

Based on the analysis conducted using ICP, the product obtained (Table 4), the ratio of Ca/F for n-CaF₂ was 0.5, it's a pure n-CaF₂ product.

Adsorption study

Effect of adsorbent amount

The effect of the adsorbent amount on RB21 removal rate was investigated, and the results are presented in Figure 6. It was observed that the decolorization yield increases with the mass of the adsorbent up to an optimum mass, beyond which the decolorization yield remains constant even with further increases in adsorbent mass. Specifically, an optimum mass of 0.8 g of CaF₂ resulted in a decolorization yield increase from 2% to 75% for RB21 (Figure 7). This phenomenon can be attributed to the increased number of sites available for dye molecule fixation

**Figure 3.** XRD data of the (111) peak for n-CaF₂ dried at 105 °C (a), calcined at 600 °C (b) and 900 °C (c)**Figure 4.** FTIR spectra of dried n-CaF₂ at 105 °C (a), calcined sample at 600 °C (b) and at 900 °C (c)

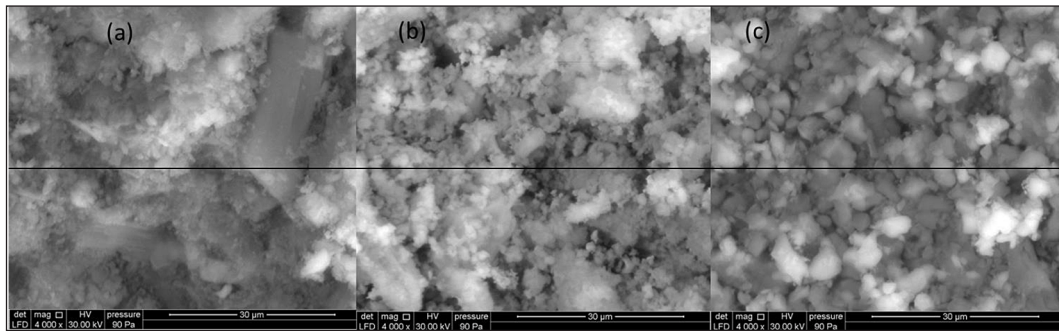


Figure 5. SEM images of n-CaF₂ dried at 105 °C (a), calcined at 600 °C (b) and 900 °C

Table 4. Chemical analysis of n-CaF₂ at 105 °C

Prepared CaF ₂	%								Pppm					
	Ca	F	Al	Fe	K	Mg	Na	Si	Ba	Mn	Ti	Pb	Sr	Zn
	50.2	47.9	0.05	0.32	0.11	0.07	0.08	0.20	41.18	0.66	705	0.96	564	1.2

with higher doses of adsorbent, thereby enhancing the adsorption process. (Aggadi et al., 2021, Cechinel et al., 2022, Shakoor et al., 2016).

Effect of pH (amount of adsorbent)

The pH of the colored solution not only affects the surface charge of the adsorbent but also influences the degree of ionization of materials, contributes to the dissociation of functional groups at the active sites of the adsorbent, and impacts the structure of adsorbent molecules. In this study, we investigated the adsorption efficiency of the adsorbent by varying the pH from 2.8 to 11.7 using either a 0.1 N hydrochloric acid (HCl) solution or a 0.1 N sodium hydroxide (NaOH) solution to achieve the desired pH

level. Under these pH conditions, a mass of 0.8 g of CaF₂ was stirred in 100 mL of the colored 20 mg/L solution. The results obtained from these tests are presented in Figure 8. The results shown in Figure 7 show that after the neutrality range the pH is strongly influences the decolorization yield, compared to the normal pH of the sample (pH = 6.4). This effect increases significantly when the pH moves away from the neutral zone. This can be explained by the protonation at acidic pH, This increase in pH enhances the electrostatic attractions between the negatively charged poles of the dye and the positively charged adsorption sites. As a result, there is a slight improvement in adsorption efficiency (Yadav et al., 2022, Longhinotti et al., 1998).

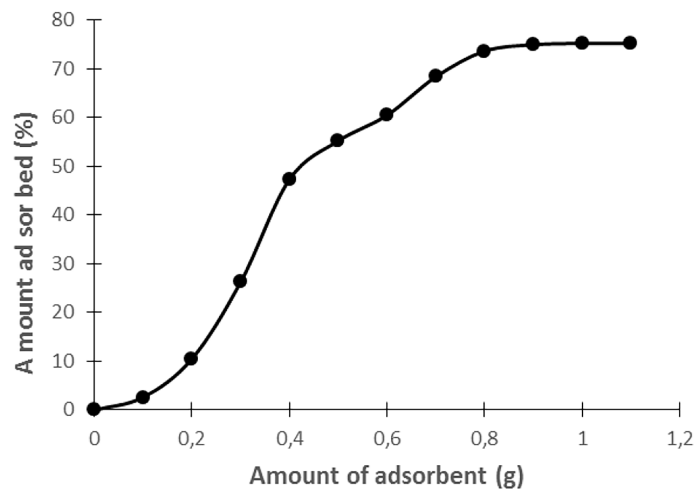


Figure 6. Effect of amount of adsorbent (CaF₂) on RB21 adsorption (C₀ = 20 mg / L; pH = 6.4; agitation = 500 rpm; V = 100 mL; contact time = 2h; T = 24 ± 2 °C)

Effect of contact time

To investigate the adsorption kinetics of the RB21 dye on the synthesized calcium fluoride (CaF_2), experiments were conducted under consistent operating conditions as described previously: using a 100 mL volume of dye solution with a concentration of 20 mg/L, stirring at 500 rpm, employing 0.8 g of calcium fluoride, and maintaining normal pH. Samples were collected at regular time intervals to measure the residual dye concentrations. The obtained results are illustrated in Figure 8.

The kinetic study of RB21 retention by the adsorbent studied shows that the decolorization yield

increases rapidly with the increase in the contact time. Equilibrium is usually reached after 80 minutes of stirring. After this contact time, the decolorization yield of the RB21 solution reaches 74%. As in the case of the study of the effect of mass, we also find that the adsorption affinity of synthesized calcium fluoride (CaF_2) is important for the removal of the anionic dye (RB21) (Dey et al., 2022).

Effect of initial dye concentration

The experiments involved stirring 0.8 g of synthesized calcium fluoride (CaF_2) for 120 minutes in dye solutions with concentrations ranging from 10 to 180 mg/L. The tests were conducted at

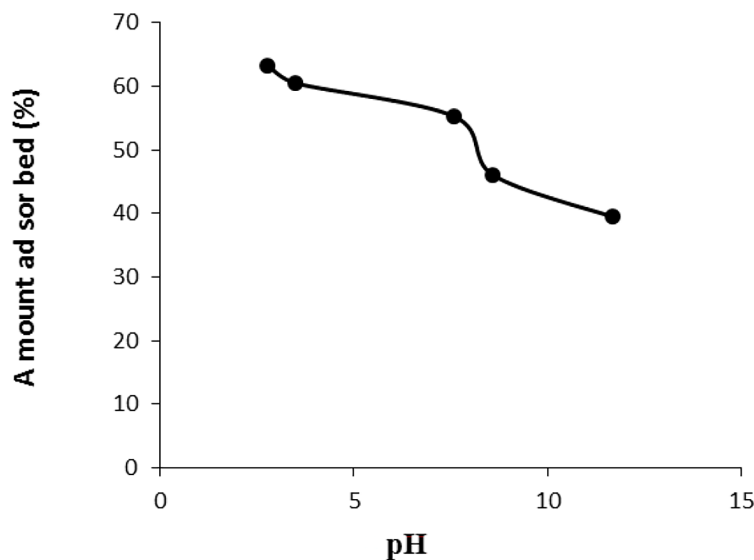


Figure 7. Decolorization of aqueous solution of RB21 by synthesized calcium fluoride as a function of pH ($V = 100$ mL; $\text{pH}_{\text{in}} = 6.4$; $C_0 = 20$ mg / L; contact time = 2h; speed agitation = 500 rpm; $T = 24 \pm 2$ °C)

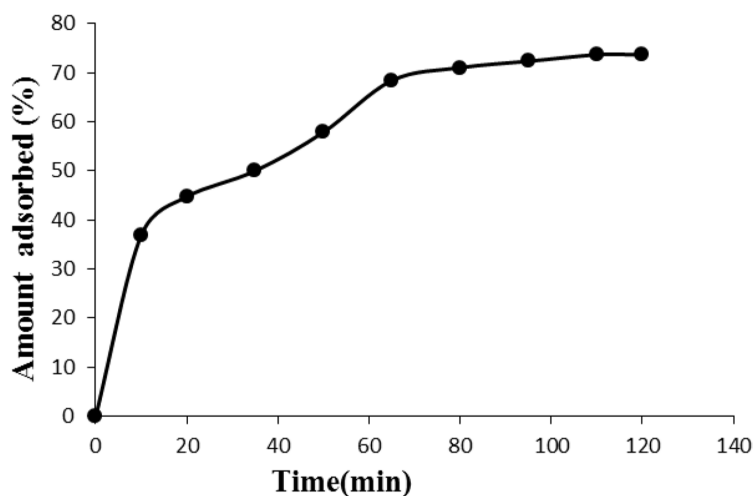


Figure 8. Effect of contact time on the adsorption of the dye (RB21) by calcium fluoride (CaF_2) ($C_0 = 20$ mg / L; $\text{pH}_{\text{in}} = 6.4$; stirring speed = 500 rpm ; $V = 100$ mL, $T = 24 \pm 2$ °C)

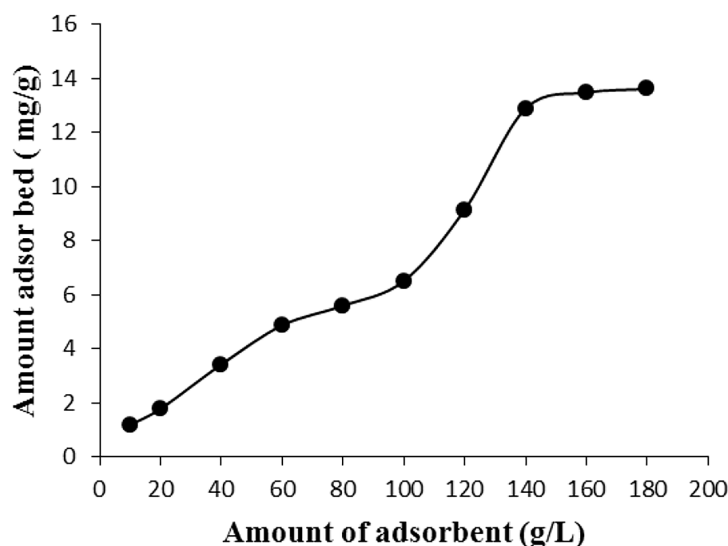


Figure 9. Effect of initial dye (RB21) concentration on the adsorption by calcium fluoride, (pH = 6.4; m = 1.2 g; V = 100 mL; contact time = 2 h; agitation = 500 rpm; T = 24 ± 2 °C)

normal pH, a stirring speed of 500 rpm, and room temperature. Residual concentrations were measured and used to assess the change in adsorption capacity relative to the initial dye concentration, as depicted in Figure 9. The results show that the adsorption capacity of synthesized calcium fluoride (CaF₂) increases with increasing initial dye concentration. Other ways, a plateau of adsorption capacity is observed at concentration of 140 mg/L. That can be explained by the saturation of the active sites of the two adsorbents in the presence of a high dye content (Boruah et al., 2022).

CONCLUSIONS

The study focuses on the synthesis of n-CaF₂ particles using the pure wet phase method, followed by a comprehensive characterization of the resulting compound through X-ray diffraction, scanning electron microscopy, and Fourier-transform infrared spectroscopy analyses. This method is particularly effective for producing materials in a pure phase, offering several advantages such as controllable size, uniform morphology and shape, a wide range of achievable compositions, and lower reaction temperatures, even at room temperature. Subsequently, the synthesized nano-CaF₂ was evaluated for its efficacy in RB21 dye adsorption, with a detailed optimization of adsorption parameters. The investigation revealed significant influences of contact time and adsorbent

dose on RB21 adsorption, with the adsorption capacity showing a notable increase with these parameters until reaching equilibrium. These findings highlight the potential of nano-CaF₂ as a highly efficient adsorbent for RB21 dye removal, showcasing its promising application in wastewater treatment processes. The characterization techniques employed, including XRD, SEM, and FTIR analyses, provided valuable insights into the structural and chemical properties of the synthesized nano-CaF₂, contributing to a comprehensive understanding of its adsorption behavior and suitability for environmental remediation applications. Overall, this study underscores the importance of innovative nanomaterial synthesis methods and their potential impact on addressing pollution challenges in water treatment.

REFERENCES

1. Alzahrani J.S., Midala I.H., Kamari H.M., Al-Hada N.M., Tim C.K., Nidzam N.N.S., Alrowaili Z.A., Al-Buriah M.S., Alrowaili Z.A., Al-Buriah M.S. 2022. Effect of calcination temperature on the structural and optical properties of (ZnO) 0.8 (ZrO₂) 0.2 nanoparticles. *J. Inorg. Organomet. Polym. Mater.*, 32, 1755–1765. <https://doi.org/10.1007/s10904-022-02238-8>
2. Bensalah A., Mortier M., Patriarcheb G., Gredin P., Vivien D. 2006. Synthesis and optical characterizations of undoped and rare. *J. Solid. State Chem.* 179, 2636–2644. <https://doi.org/10.1016/j.jssc.2006.05.011>

3. Bhadane M.S., Gavhane K.H., Ghemud V.S., Deshmukh S.B., Bagekari Y.G., Kulkarni P.P., Dahiwale S.S., Bhoraskar V.N., Dhole S.D. 2023. 6 MeV electron beam induced TL dosimetric properties of CaF₂: Dy nanophosphor. *Opt. Mater.* 136, 113452. <https://doi.org/10.1016/j.optmat.2023.113452>
4. Boruah. T., Das S.K., Kumar G., Mondal S., and Dey R.S. 2022 Dual active sites in a triazine-based covalent organic polymeric framework promoting oxygen reduction reaction. *Chem. Comm.* 58(36), 5506–5509. <https://doi.org/10.1039/D2CC00865C>
5. Cechinel M.A.P., de Guidolin T.O., da Silveira A.R., Tasca J.S., Montedo O.R.K. 2022. Coal mining pyritic waste in Fenton-like processes: Raw and purified catalysts in Reactive Blue 21 dye discoloration. *Sci. Total Environ.* 807, 150823 <https://doi.org/10.1016/j.scitotenv.2021.150823>
6. Dey N., Kamatchi C., Vickram A.S., Anbarasu K., Thanigaivel S., Palanivelu J., Pugazhendhi A., Ponusamy V.K. 2022. Role of nanomaterials in deactivating multiple drug resistance efflux pumps—A review. *Environ. Res.*, 204, 111968. <https://doi.org/10.1016/j.envres.2021.111968>
7. Fosca M., Rau J.V., Uskoković V. 2022. Factors influencing the drug release from calcium phosphate cements. *Bioactive Materials*, 7, 341–363. <https://doi.org/10.1016/j.bioactmat.2021.05.032>
8. Fujihara S., Kadota Y., Kimura T. 2002. Role of organic additives in the sol-gel synthesis of porous CaF₂ anti-reflective coatings. *J. Sol-Gel Sci. Technol.*, 24, 147–154. <https://doi.org/10.1023/A:1015252010509>
9. Gerward L., Olsen J.S., Steenstrup S., Malinowski M., Åsbrink S. and Waskowska A. 1992. A X-ray diffraction investigations of CaF₂ at high pressure. *J. Appl. Crystallogr.*, 25, 578–581. <https://doi.org/10.1107/S0021889892004096>
10. Golubchikov D., Safronova T.V., Nemygina E., Shatalova T.B., Tikhomirova I.N., Roslyakov I.V., Khayrutdinova D., Platonov V., Boytsova O., Kaimonov M., Firsov D.A., and Lyssenko K.A. 2023. Powder synthesized from aqueous solution of calcium nitrate and mixed-anionic solution of orthophosphate and silicate anions for bioceramics production. *Coatings*, 13, 2, 374. <https://doi.org/10.3390/coatings13020374>
11. Grass R.N., Stark W.J. 2005. Flame synthesis of calcium-, strontium-, barium fluoride nanoparticles and sodium chloride, *Chem Commun* 13, 1767–1769 <https://doi.org/10.1039/B419099H>
12. Jang J.H., Oh S., Kim H.J., Kim D.S. 2023. Randomized clinical trial for comparing the efficacy of desensitizing toothpastes on the relief of dentin hypersensitivity. *Sci. Rep.*, 13(1), 5271. <https://doi.org/10.1038/s41598-023-31616-6>
13. Kumar G.A., Chen C.W., Ballato J., Riman R.E. 2007. Optical characterization of infrared emitting rare-earth-doped fluoride nanocrystals and their transparent nanocomposites. *Chem. Mater.*, 19, 1523–1528. <https://doi.org/10.1021/cm051567n>
14. Kumar A., Sharma M., Vaish R. 2022. Screen printed calcium fluoride nanoparticles embedded antibacterial cotton fabric. *Mater. Chem. Phys.*, 288, 126449. <https://doi.org/10.1016/j.matchemphys.2022.126449>
15. Lebkiri I., Abbou B., Hsissou R., Safi Z., Sadiku M., Berisha A., El Amri A., Essaadaoui Y., Kadiri L., Lebkiri A., Rifi E.H. 2023. Investigation of the anionic polyacrylamide as a potential adsorbent of crystal violet dye from aqueous solution: Equilibrium, kinetic, thermodynamic, DFT, MC and MD approaches. *J. Mol. Liq.* 372, 121220. <https://doi.org/10.1016/j.molliq.2023.121220>
16. Longhinotti E., Pozza F., Furlan L., Sanchez M.N.M., Klug M., Laranjeira M.C.M., Fávere V.T. 1998. Adsorption of anionic dyes on the biopolymer chitin. *J. Braz. Chem. Soc.*, 9, 435–440. <https://doi.org/10.1590/S0103-50531998000500005>
17. Matsuo S., Rölla G., Lagerlöf F. 1990. Effect of fluoride addition on ionized calcium in salivary sediment and in saliva containing various amounts of solid calcium fluoride. *Eur. J. Oral. Sci.*, 98, 482–485. <https://doi.org/10.1111/j.1600-0722.1990.tb01002.x>
18. Mayerhöfer T.G., Pahlow S., Hübner U., Popp J. 2020. CaF₂: An ideal substrate material for infrared spectroscopy. *Anal. Chem.*, 92, 9024–9031. <https://doi.org/10.1021/acs.analchem.0c01158>
19. Mitwalli H., Al Sahafi R., Alhussein A., Oates H.W., Melo M.A.S., Xu H.H.K., Weir M.D. 2022. Novel rechargeable calcium fluoride dental nanocomposites. *Dent. Mater.*, 38, 397–408. <https://doi.org/10.1016/j.dental.2021.12.022>
20. Mortier M., Bensalah A., Dantelle G., Patriarche G., Vivien D. 2007. Doped oxyfluoride glass-ceramics and fluoride ceramics: Synthesis and optical properties. *Opt. Mater.*, 29, 1263–1270. <https://doi.org/10.1016/j.optmat.2005.12.014>
21. Motameni A., Alshemary A.Z., Evis Z.A. 2021. Review of synthesis methods, properties and use of monetite cements as filler for bone defects. *Cera. Int.*, 47, 13245–13256. <https://doi.org/10.1016/j.ceramint.2021.01.240>
22. Nasrellah H., Yassine I., Hatimi B., Joudi M., Chemaa A., El Gaini L., Hatim Z., El Mhammedi M.A., Bakasse M. 2017. Nouvelle synthèse d'hydroxyapatite à partir de phosphogypse local. *JMES*, 8(9), 3168–3174.
23. Nasrellah H., Joudi M., Bensemali M., Yassine I., Hatimi B., Hafdi H., Mouldar J., El Mhammedi M.A. and Bakasse M. 2022. Novel synthesis and characterization of crystalline fluorapatite from Moroccan phosphogypsum waste. *Matériaux & Techniques*, 110(1), 102.

- <https://doi.org/10.1051/mattech/2022007>
24. Yassine I., Joudi M., Hafdi H., Hatimi B., Mouldar J., Bensemlali M., Nasrellah H., El Mahammedi M.A., Bakasse M. 2022. Synthesis of brushite from phosphogypsum industrial waste. *Biointerface Research in Applied Chemistry*, 12(5), 6580–658815. <https://doi.org/10.33263/BRIAC125.65806588>
 25. Bensemlali M., Joudi M., Nasrellah H., Yassine I., Aarfane A., Hatimi B., Hafdi H., Mouldar J. and Bakasse M. 2022. One-step synthesis and characterization of crystalline nano-calcite from phosphogypsum by precipitation method. *The European Physical Journal Applied Physics*, 97, 50. <https://doi.org/10.1051/epjap/2022220041>
 26. Rølla G., Saxegard E. 1990. Critical evaluation of the composition and use of topical fluorides with emphasis on the role of calcium fluoride in caries inhibition. *J. Dent. Res.*, 69, 780–785. <https://doi.org/10.1177/00220345900690S150>
 27. El Aggadi S., El Hourch A. 2021. Removal of Reactive Blue 21 (RB21) Phthalocyanine Dye from Aqueous Solution by Adsorption Process. *J. Environ. Stud.*, 30, 3425–3432. <https://doi.org/10.15244/pjoes/127384>
 28. Shakoor H., Ibrahim M., Usman M., Adrees M., Mehmood M.A., Abbas F., Rasool N., Ibrahim M. 2016. Removal of reactive blue 21 from aqueous solution by sorption and solubilization in micellar media. *J. Dispers Sci. Technol.*, 37, 144. <https://doi.org/10.1080/01932691.2015.1035387>
 29. Sun X., Li Y. 2003. Nanocubes de CaF₂ monocristallins luminescents à taille variable. *Chem. Commun.*, 14, 1768–1769. <https://doi.org/10.1039/B303614F>
 30. Takaya Y., Inoue S., Kato T., Fuchida S., Tsujimoto S., Tokoro C. 2021. Purification of calcium fluoride (CaF₂) sludge by selective carbonation of gypsum. *J. Environ. Chem. Eng.*, 9, 104510. <https://doi.org/10.1016/j.jece.2020.104510>
 31. Wang L., Wang B., Wang X., Liu W. 2007. Tribological investigation of CaF₂ nanocrystals as grease additives. *Tribol. Int.*, 40, 1179–1185. <https://doi.org/10.1016/j.triboint.2006.12.003>
 32. Wang M., Ye H., Zheng X., Chen S., Xing H., Tao X., Dang Z., Lu G. 2023. Adsorption behaviors and mechanisms of simultaneous cadmium and fluoride removal on waste bovine bone from aqueous solution. *J. Environ. Chem. Eng.*, 11(1), 109035. <https://doi.org/10.1016/j.jece.2022.109035>
 33. Wu Y., Mayer J.T., Garfunkel E., Madey T.E. 1994. X-ray photoelectron spectroscopy study of water adsorption on BaF₂ (111) and CaF₂ (111) surfaces. *Langmuir*, 10, 1482–1487 <https://doi.org/10.1021/la00017a027>
 34. Yadav B.S., Dasgupta S. 2022. Effect of time, pH, and temperature on kinetics for adsorption of methyl orange dye into the modified nitrate intercalated MgAl LDH adsorbent. *Inorg. Chem. Commun.*, 137, 109203. <https://doi.org/10.1016/j.inoche.2022.109203>
 35. Young A.M., Ng P.Y.J., Gbureck U., Nazhat S.N., Barralet J.E., Hofmann M.P. 2008. Characterization of Chlorhexidine-Releasing, Fast-Setting, brushite Bone Cements. *Acta. Biomater.*, 4, 1081–1088. <https://doi.org/10.1016/j.actbio.2007.12.009>
 36. Zhou H., Yang L., Gbureck U., Bhaduri S.B., Sikder P. 2021. An important calcium phosphate compound—its synthesis, properties and applications in orthopedics. *Acta Biomater*, 127, 41–55. <https://doi.org/10.1016/j.actbio.2021.03.050>
 37. Zhou L., Chen D., Luo W. 2007. Transparent glass ceramic containing Er³⁺:CaF₂ nano-crystals prepared by sol-gel method. *Mater. Lett.*, 61, 3988–3990. <https://doi.org/10.1016/j.matlet.2007.01.001>
 38. Zsigmondy R., Scherrer P. 1912. Bestimmung der inneren Struktur und der Größe von Kolloidteilchen mittels Röntgenstrahlen. *Kolloidchemie. Kolloidchemie Ein. Lehrbuch*. 387–409. https://doi.org/10.1007/978-3-662-33915-2_7